JACS
JOURNAL OF THE AMERICAN CHEMICAL SOCIETY
pubs.acs.org/JACS
Article

Origin of the ^{31}P NMR Chemical Shift in Lewis Acid Adducts of Triethylphosphine Oxide. Does the Gutmann–Beckett Method Relate to Lewis Acid Strength?

Alexander A. Kolganov, Maximillian Kling, Matthew P. Conley,* and Evgeny A. Pidko*

Cite This: J. Am. Chem. Soc. 2026, 148, 14768–14778
Read Online

ACCESS | Metrics & More | Article Recommendations | Supporting Information

ABSTRACT: The Gutmann–Beckett method involves the reaction of a phosphine oxide with a Lewis acid, followed by measurement of the change in ^{31}P NMR chemical shift ($\Delta\delta$) relative to the free phosphine oxide. This is the most commonly used experimental method to assess Lewis acid strength in solution and on solid materials containing Lewis acid sites. This study describes the origin of the ^{31}P NMR $\Delta\delta$ deshielding that occurs in triethylphosphine oxide (TEPO) adducts of Lewis acids. 57 Lewis acid adducts were studied using DFT methods. These models span typical three-, four-, and five-coordinate Lewis acids as well as models that approximate the coordination sphere of Lewis acid sites proposed to be present in heterogeneous materials. When a TEPO···Lewis acid adduct forms, electron density from the oxygen is transferred to the Lewis acid, which reduces the negative hyperconjugation from the oxygen to the σ^*_{P-C} that weakens the P═O bond. Experimental and DFT studies show that the ^{31}P NMR chemical shift deshields in TEPO···Lewis adducts because the most shielded δ_{33} component of the chemical shift tensor shifts dramatically downfield. This deshielding is correlated with the weakening of the P═O bond. Natural chemical shift (NCS) analysis shows that δ_{33} deshielding in Lewis acid adducts is due to coupling of the filled σ_{P-C} with the empty $\pi^*_{P=O}$, the LUMO of the TEPO fragment. This study connects the ^{31}P NMR chemical shift, in particular the experimentally observable $\Delta\delta_{33}$, to P═O bond weakening. Thus, the Gutmann–Beckett method does not provide information on adduct formation energy, the more typically sought measure of Lewis acidity, but rather provides a different thermodynamic descriptor of Lewis acid strength in the weakening of the P═O bond.

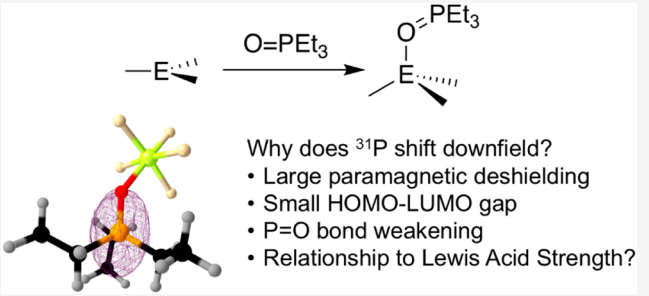

INTRODUCTION

Lewis acids contain low lying empty orbitals that can accept electron density from substrates.[1] This critically important interaction polarizes the bound substrate and facilitates further chemical reactivity. This model is used widely throughout organic synthesis to mediate bond forming reactions and to build molecular complexity.[2] At the extreme, when a Lewis acid and Lewis base are too bulky to form the classical adduct, frustrated Lewis pair (FLP) behavior emerges, enabling activation of inert bonds, such as activation of the H–H bond in dihydrogen.[3] Importantly, such reactivity can be achieved with main-group (often nonmetal) components, positioning FLPs as catalysts for transformations typically mediated by transition metals.[4]

Similar scenarios arise in materials that contain strong Lewis sites that are broadly important in heterogeneous catalysis.[5] For example, aluminum oxide (Al_2O_3) is proposed to contain a low quantity of strong Lewis acid Al-sites that activate N_2 or C–H bonds.[6] These reactive sites may also play a role in generation of organometallic ion-pairs that form on Al_2O_3 supports.[7] $AlCl_xF_{3-x}$ is proposed to contain stronger Lewis sites than Al_2O_3, which react with R_3SiH to form electrophilic silylium-like intermediates that activate C–F bonds.[8] Discrete silylium-like ions supported on weakly coordinating oxides show similar reactivity.[9]

Strong Lewis acids are also involved in reactions catalyzed by metal-exchanged zeolites[10] or amorphous oxides containing well-defined metal sites.[11] These materials can coordinate and heterolytically split aliphatic C–H bonds,[12] resulting in organometallic intermediates that are relevant to propane dehydrogenation,[12c,13] and ethylene polymerization.[14] Though limited, this set of examples points to Lewis acidity as the unifying motif across reactivity encountered in solution and on surfaces.

The ability to control the reactivity of a Lewis acid is related to its strength. IUPAC defines Lewis acid strength as a measure of, "the equilibrium constants for Lewis adduct formation of a series

Received: October 7, 2025
Revised: February 25, 2026
Accepted: March 10, 2026
Published: April 1, 2026

of Lewis acids with a common reference Lewis base."[15] In practice, a common experimental method to assess Lewis acid strength was proposed by Gutmann and Beckett, which involves the reaction of a Lewis acid with triethylphosphine oxide (TEPO) (eq 1).[16,17] TEPO often binds irreversibly to strong

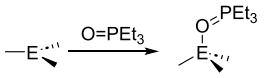

(1)

Lewis acids, and the resulting change in the isotropic ^{31}P NMR chemical shift ($\Delta\delta_{iso}$) of the diamagnetic adduct relative to free TEPO is widely taken as a measure of Lewis acid strength. Care must be taken to ensure that the ^{31}P NMR chemical shift measured in solution is representative of the static TEPO adduct and not affected by exchange between free and complexed TEPO.[17,18]

This method is broadly applied in solution and to solids containing strong Lewis or Brønsted acid sites.[19] Lewis sites present on heterogeneous surfaces are obviously impossible to isolate and study crystallographically, thus indirect probes are essential to assess their Lewis acid strength. The Gutmann–Beckett method is very convenient for this purpose because solid-state ^{31}P{^{1}H} MAS NMR spectra are generally easy to acquire. Additionally, TEPO adsorbed on surfaces does not generally engage in equilibria and/or solvent dependent dynamic behavior that can complicate studies in solution.[20]

However, $\Delta\delta_{iso}$ values across chemically diverse Lewis acids correlate poorly with calculated energies for adduct formation,[17] suggesting that this method may not directly probe Lewis acid strength. In contrast, Brønsted acid strength correlates quite well with $\Delta\delta_{iso}$ of TEPO.[21] In the absence of water, protons form linear hydrogen bond adducts with anions and/or hydrogen bond acceptors.[22] TEPO is an H-bond acceptor and forms TEPO···H···X$^-$, where X$^-$ is the conjugate base of the HX acid. The key difference between TEPO···H···X$^-$ and TEPO···LA is that a Lewis acid must undergo structural distortion to form the adduct that is a significant component of binding energy (ΔE_{bind}) in this reaction. Erdmann and Greb proposed that ΔE_{bind} should be viewed as the sum of the unfavorable deformation energy (E_D) to distort the Lewis acid and the favorable interaction energy (E_I) to form the adduct (eq 2).[17] This treatment gives a good correlation between calculated E_I and $\Delta\delta_{iso}$ (R^2 = 0.81).[17]

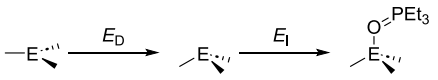

(2)

The NMR chemical shift relates to electronic structure,[23] thus $\Delta\delta_{iso}$ values are reporting changes in electronic structure at phosphorus in TEPO···Lewis adducts. We set out to determine the origin of $\Delta\delta_{iso}$ in a broad set of Lewis acids shown in Figure 1. These span typical three-, four-, and five-coordinate Lewis acids to more modern Al(OR^F)$_3$ (OR^F = C(CF$_3$)$_3$),[24] B(*o*Cb)$_3$ (*o*Cb = *ortho*-carborane),[25] or HB^{Me}*o*Cb$_2$.[26] This study also includes cationic Lewis acids, including carbocations, silylium, germylium, stannylium, B(Mes)$_2^+$,[27] and Sb(C$_6$F$_5$)$_4^+$;[28] as well as transition metal containing Lewis acids. Eight surface models extend the analysis to representative Lewis acidic motifs in heterogeneous catalysts. These include models that approximate the coordination environment of strong aluminum[29] or boron[30] Lewis acids supported on amorphous silica, the pyrosulfate supported on zirconium oxide,[31] and four cluster models of metal-exchanged zeolite models in the BEA topology.[32] This breadth allows us to test the generality of the Gutmann–Beckett metric across chemically diverse bonding regimes and environments. Our analysis reveals that $\Delta\delta_{iso}$ primarily reflects adduct-induced polarization of the TEPO P=O bond, rather than the intrinsic strength of the TEPO···Lewis acid interaction.

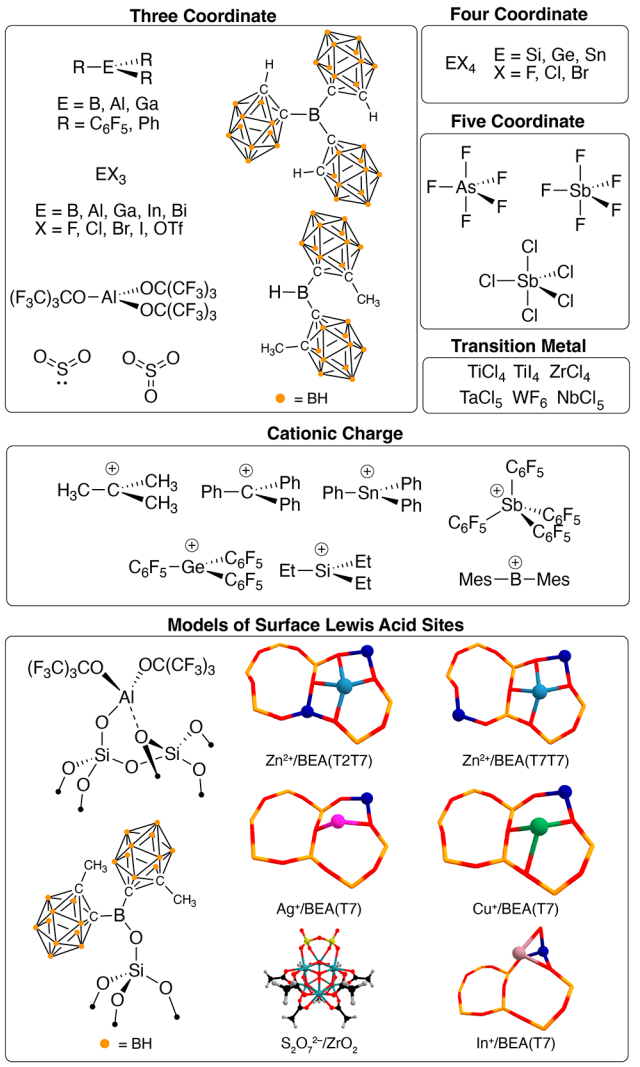

Figure 1. Lewis acids studied here.

RESULTS AND DISCUSSION

Energetics of TEPO Adduct Formation

Figure 2 shows the natural localized molecular orbitals (NLMOs)[33] that describe the bonding between phosphorus and oxygen in TEPO in NBO 7.0 formalism.[34] The σ_{P-O} (not shown) is a dative σ bond originating from donation of the nonbonding lone pair on phosphorus to oxygen that completes the octet and results in three lone pairs on O. The n_1(O) lone pair is colinear with the P–O bond and is localized on oxygen with high s-character (64% s, 36% p). Two lone pairs, n_2(O) and n_3(O), orient roughly perpendicular to the P–O bond axis and donate electron density to their respective σ^*_{P-C} antibonding orbitals (Figure 2a). These NLMOs display occupancy on both the oxygen and the corresponding antibonding P–C regions. This analysis is in agreement with previous computations,[35] and is referred to as negative hyperconjugation.[36]

https://doi.org/10.1021/jacs.5c17621
J. Am. Chem. Soc. 2026, 148, 14768–14778

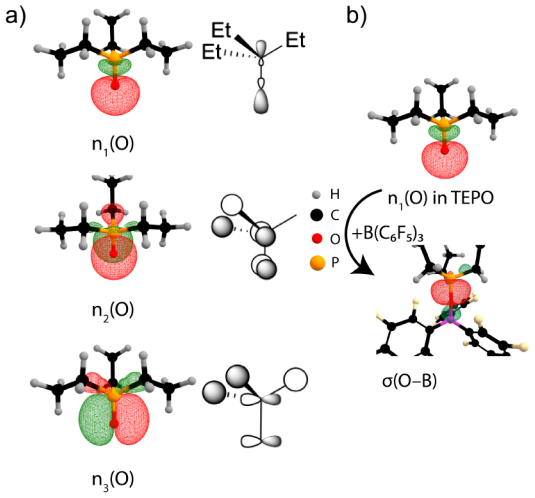

Figure 2. (a) Natural-localized molecular orbital (NLMO) plots of negative hyperconjugation in free TEPO. ChemDraw sketches of these orbitals are given next to the NLMO plots. (b) Coordination to $B(C_6F_5)_3$ converts the $n_1(O)$ lone pair into an O → B σ-bond.

To streamline the discussion, we will largely focus on free TEPO and the representative TEPO···$B(C_6F_5)_3$ adduct to illustrate how a Lewis acid perturbs the electronic structure at phosphorus, and to show how this relates to the ^{31}P NMR chemical shift. Other Lewis acids shown in Figure 1 follow the trends described below for TEPO and the TEPO···$B(C_6F_5)_3$ adduct. All relevant data for those Lewis acids is summarized in the Section S7 of the Supporting Information.

The $n_1(O)$ lone pair is responsible for adduct formation with Lewis acids. At the ωB97M-D3BJ/def2-TZVPP level of theory the calculated binding energy (ΔE_{bind}) in TEPO···$B(C_6F_5)_3$ adduct is −28.2 kcal mol^{-1} (Table 1). From eq 2, ΔE_{bind} should be viewed as the sum of the distortion energy (E_D) and the interaction energy (E_I). The optimized structure of TEPO···$B(C_6F_5)_3$ has a B−O−P bond angle of 156.1°, close to the experimentally observed 161.0°.[37] The NLMO describing this interaction is shown in Figure 2b.

Table 1. Calculated Binding (ΔE_{bind}) and Deletion ($\Delta E^{(del)}$) Energies for TEPO TEPO···$B(C_6F_5)_3$[a]

	ΔE_{bind}	$\Delta E^{(del)}_{n_x(O)\to 3\times\sigma*(P-C)}$				$\Delta E^{(del)}_{O\to\{P,C\}}$[d]
Compound		1[b]	2[b]	3[b]	all[c]	
TEPO	-	2.0	35.9	37.7	86.3	182.2
TEPO·$B(C_6F_5)_3$	−28.2	-	19.9	20.7	44.1	93.4

[a]All Energies are in kcal mol^{-1}. [b]Deletion energies for removal of individual n(O) orbitals. [c]Combined deletion energy when all n(O) orbitals are removed. [d]Deletion energy for all donor−acceptor interactions from O to the P and C atoms bonded to P.

The σ donation from O to B reduces lone pair/lone pair repulsion and weakens the negative hyperconjugation from $n_2(O)$ and $n_3(O)$. Quantitatively, this effect can be assessed with deletion energies ($\Delta E^{(del)}$) using eq 3:

$$\Delta E^{(del)}_{i,j} = E[F^{(i,j)} = 0] - E[F^{(full)}] \quad (3)$$

$\Delta E^{(del)}$ is the total energy increase when selected Fock matrix elements ($F^{(i,j)}$) corresponding to selected donor−acceptor couplings are removed followed by a full SCF recalculation of the electronic structure at fixed geometry.[38]

We calculated two types of energy deletions:

a) $\Delta E^{(del)}_{n_x(O)\to 3\times\sigma*(P-C)}$ is the individual lone pair deletion energy from removal of the donor−acceptor interactions between an oxygen lone pair ($n_1(O)$, $n_2(O)$, or $n_3(O)$) and the three σ*(P−C) antibonding orbitals. This provides a selective measure of the n(O) → σ*(P−C) hyperconjugative stabilization. Combined lone pair deletion energy from the simultaneous removal of all oxygen lone pair donor−acceptor interactions to σ*(P−C) orbitals was also calculated because individual deletion energies are nonadditive.

b) $\Delta E^{(del)}_{O\to\{P,C\}}$ is the deletion energy of all Fock matrix elements between the oxygen atom and the phosphorus/carbon atoms bonded to P. This removes all occupied → vacant orbital interactions originating from oxygen and terminating at P or the three carbon atoms, which removes the total influence of oxygen lone pair delocalization on molecular stability and includes n(O) → σ*(P−C) delocalization.

In the case for free TEPO, the combined lone pair deletion energy 86.3 kcal mol^{-1}, with the nearly identical contributions from $n_2(O)$ and $n_3(O)$ of 35.9 and 37.7 (Table 1). The formation of TEPO···$B(C_6F_5)_3$ adduct results in a significant reduction of the n(O) → σ*(P−C) delocalization, as is evidenced from the decrease of the combined deletion energy to 44.1 kcal mol^{-1} as well as the individual contributions from $n_2(O)$ and $n_3(O)$ (19.9 and 20.7 kcal mol^{-1}, respectively). This result indicates, somewhat unsurprisingly, that Lewis acid coordination to TEPO results in P═O bond weakening, which is a thermochemical descriptor of Lewis acid strength.

As expected, $\Delta E^{(del)}_{O\to\{P,C\}}$ for TEPO is larger than the combined lone pair delocalization because it captures additional minor channels beyond n(O) → σ*(P−C). Nevertheless, this interaction remains dominant, as evidenced by the orbital occupancy changes upon deletion. The natural populations of $n_2(O)$ and $n_3(O)$ each increase by 0.18 electrons, while the three σ*(P−C) orbitals each decrease by 0.09 electrons; all other orbital population shifts are ≤ 0.01 electrons. This confirms that n(O) → σ*(P−C) hyperconjugation accounts for the majority of the stabilization captured by deletion. For the analysis presented below we use $\Delta E^{(del)}_{O\to\{P,C\}}$ because this is the most inclusive descriptor of negative hyperconjugative interactions in the phosphine oxide adducts. (Figure S5.4) $\Delta E^{(del)}_{O\to\{P,C\}}$, and related individual and combined deletion energies for all adducts are given in the Supporting Information (Table S7.1).

In all adducts ΔE_{bind} are all exoergic and $\Delta E^{(del)}_{O\to\{P,C\}}$ values decrease relative to free TEPO. There is no obvious correlation between ΔE_{bind} and $\Delta E^{(del)}_{O\to\{P,C\}}$ (Figure S4.1b) The strongest Lewis acid in this series in terms of ΔE_{bind} is the Zn^{2+}/BEA (T7T7) model (ΔE_{bind} = −81.2 kcal mol^{-1}). The large ΔE_{bind} does not imply a more pronounced weakening of the coordinated P═O bond. The $\Delta E^{(del)}_{O\to\{P,C\}}$ energy in TEPO···Zn^{2+}/BEA (T7T7) is 93.6 kcal mol^{-1}, close to $\Delta E^{(del)}_{O\to\{P,C\}}$ of $B(C_6F_5)_3$.

The primary coordination sphere of the Zn^{2+} ion in the Zn^{2+}/BEA (T7T7) is shown in Figure 3a. Zinc is in a distorted square

https://doi.org/10.1021/jacs.5c17621
J. Am. Chem. Soc. 2026, 148, 14768−14778

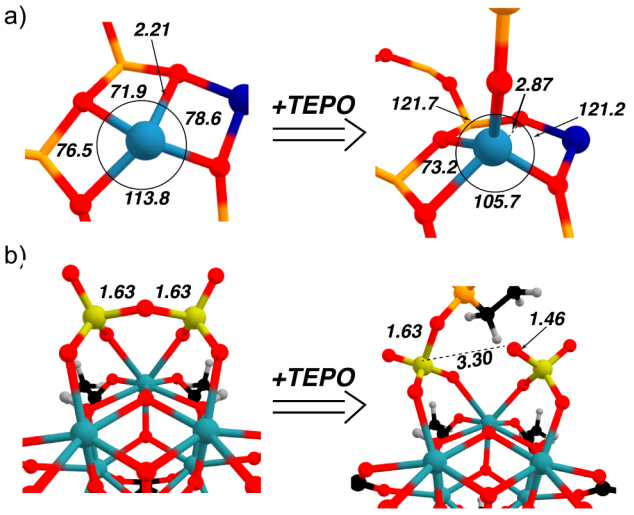

Figure 3. Local structures of Zn^{2+}/BEA (T7T7) (a) and $S_2O_7^{2-}/ZrO_2$ cluster (b) and their TEPO adducts. Important bond angles and distances (in Å) are listed in the figure.

planar coordination environment, displaced from the plane defined by the four oxygens by 0.50 Å. One Zn−O bond is significantly longer than the other three Zn−O bonds, suggesting this bond is weaker than the other three. The Lewis acidity of the Zn^{2+} center is further enhanced because one of the two charge-compensating AlO_4^- tetrahedra resides in an adjacent ring rather than in the ring directly coordinating Zn^{2+}. As a result, the positive charge on zinc is less effectively compensated, and the metal coordinates predominantly to less basic Si−O−Si oxygens rather than Si−O−Al ones. A molecular analogy could be zinc salen complexes, which also adopt distorted square planar coordination environments and are strong Lewis acids that readily bind a fifth ligand in supramolecular assemblies.[39]

Coordination of TEPO results in three similar Zn−O bond distances to the zeolitic framework and O−Zn−O bond angles near tetrahedral values. The weak Zn−O bond in Zn^{2+}/BEA (T7T7) is no longer present, the distance between zinc and this oxygen increases to 2.87 Å. These results explain why ΔE_{bind} is large and $\Delta E^{(del)}_{O\rightarrow\{P,C\}}$ is small. The distorted square planar Zn^{2+} center is a strong Lewis acid that relaxes to the more common, and less Lewis acidic, tetrahedral zinc when TEPO coordinates to the metal. Another aspect that likely contributes to the large ΔE_{bind} is relaxation of the strained 5-membered ring. TEPO coordination also results in O−Al−O bond angle relaxing from 91.1° in Zn^{2+}/BEA (T7T7) to 100.0°, the latter of which is closer to tetrahedral values associated with SiO_x and AlO_x nodal points in zeolitic materials.

A small ΔE_{bind} does not imply the P═O bond is strong (e.g., large $\Delta E^{(del)}_{O\rightarrow\{P,C\}}$ energies). The $S_2O_7^{2-}/ZrO_2$ cluster (Figure 3b) has ΔE_{bind} of only −12.8 kcal mol^{-1}, but very small $\Delta E^{(del)}_{O\rightarrow\{P,C\}}$ energy of 58.3 kcal mol^{-1}, the lowest in the series studied here. This adduct forms by opening the pyrosulfate to form a sulfate anion and SO_3 bound to Zr that coordinates to TEPO.[31] In this case the ΔE_{bind} is a composite of S−O bond breaking (endothermic) and S−O═P bond making (exothermic), which likely contributes to the low binding energy using this model.

The calculated TEPO adducts adopt a range of structures that contain E−O−P bond angles ranging from 179.8° to 110.8°. There is no obvious trend in the data connecting the E−O−P bond angles to $\Delta E^{(del)}_{O\rightarrow\{P,C\}}$ or the ^{31}P NMR $\Delta\delta_{\text{iso}}$ discussed later. Because of the large range of E−O−P bond angles, about half of the adducts contain three lone pairs from NLMO analysis; the third lone pair is assigned to $n_1(O)$ from TEPO that is not completely transferred to the Lewis acid.

Adducts with linear E−O−P bond angles (>175°, $AlPh_3$, $B(oCb)_3$, $Sb(C_6F_5)_4^+$, $Ge(C_6F_5)_3^+$, and TiI_4) are essentially C_{3v} symmetric. The $n_1(O)$ lone pair donates to an empty orbital on the Lewis acid and the individual lone pair energies for $n_2(O)$ and $n_3(O)$ are nearly degenerate. However, there are weak interactions between $n_2(O)$ and $n_3(O)$ and the Lewis acid. The NLMOs for $n_2(O)$ and $n_3(O)$ in TEPO···$Ge(C_6F_5)_3^+$ are shown in Figure 4a, showing that both donate electron density to low-lying σ^* orbitals on germanium. NBO analysis shows that $n_3(O)$ has 11% Ge characters.

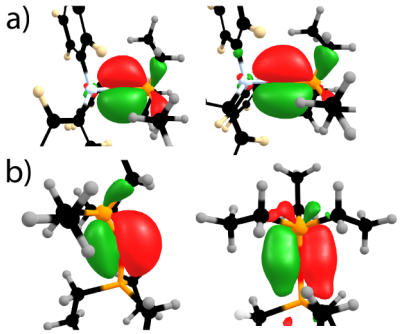

Figure 4. NLMO plots of $n_2(O)$ (left) and $n_3(O)$ (right) for $Ge(C_6F_5)_3^+$ (a) and Et_3Si^+ (b).

As the E−O−P bond angle contracts one large ($n_2(O)$) and one small ($n_3(O)$) lone pair deletion energy is obtained. In most cases, $n_3(O)$ also interacts with the Lewis acid. Figure 4b shows the $n_2(O)$ and $n_3(O)$ NLMOs for TEPO···Et_3Si^+. The $n_3(O)$ interacts with σ^* orbitals, but $n_2(O)$ orients away from the σ^* orbitals in Et_3Si^+. NBO analysis shows that $n_3(O)$ contains 12% silicon character. This trend extends to the other Lewis acids in our extended data set (Figure 1), and explains why there is one large and one small lone pair deletion energy for the π-orbital lone pairs in TEPO adducts. There are a few exceptions, however. First, due to geometric restriction in Ag^+/BEA, Cu^+/BEA, and In^+/BEA, TEPO orients $n_3(O)$ to the Lewis site in the adduct, leaving $n_1(O)$ unperturbed (Figure S6.1). Second, transition metals accept electron density from these orbitals with empty d_π orbitals, as expected.

Origin of the ^{31}P NMR Chemical Shift in Free TEPO and TEPO Adducts

For an NMR active nucleus, the chemical shift is derived from a second rank tensor (δ_{11}, δ_{22}, δ_{33}) that averages in solution due to rapid tumbling to give the isotropic chemical shift ($\delta_{iso} = (\delta_{11} + \delta_{22} + \delta_{33})/3$). These terms are directly related to shielding (σ_{ii}) experienced by the nucleus, referenced to a standard (σ^{iso}) using eq 4:

$$\begin{vmatrix} \delta_{11} & 0 & 0 \\ 0 & \delta_{22} & 0 \\ 0 & 0 & \delta_{33} \end{vmatrix} = \sigma_{iso}^{ref} \begin{vmatrix} 1 & 0 & 0 \\ 0 & 1 & 0 \\ 0 & 0 & 1 \end{vmatrix} - \begin{vmatrix} \sigma_{11} & 0 & 0 \\ 0 & \sigma_{22} & 0 \\ 0 & 0 & \sigma_{33} \end{vmatrix} \quad (4)$$

https://doi.org/10.1021/jacs.5c17621
J. Am. Chem. Soc. 2026, 148, 14768−14778

The $^{31}P\{^{1}H\}$ magic angle spinning (MAS) NMR spectrum of TEPO and TEPO···$B(C_6F_5)_3$ is shown in Figure 5 and Table 2

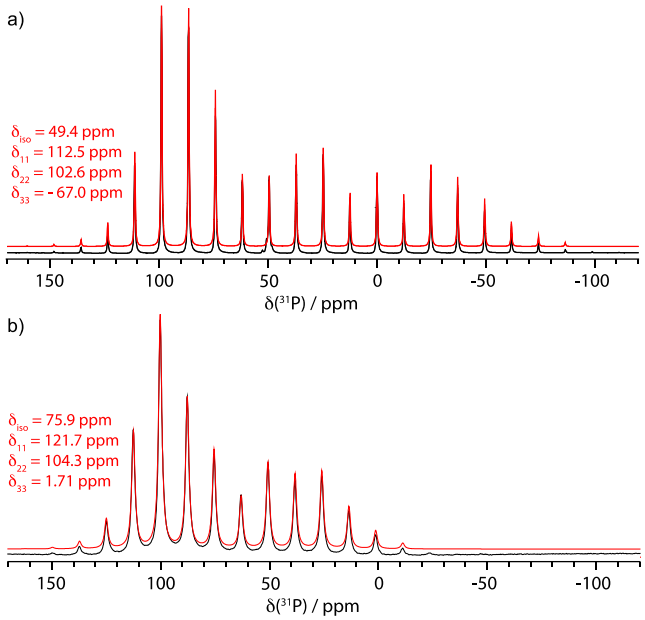

Figure 5. $^{31}P\{^{1}H\}$ MAS NMR spectra TEPO (a) and TEPO··· $B(C_6F_5)_3$ (b). The experimental data is shown in black, and the simulated spectrum is shown in red.

Table 2. Experimental and Calculated NMR Parameters for TEPO and TEPO···$B(C_6F_5)_3$ Reported in ppm

	Compound	δ_{iso}	δ_{11}	δ_{22}	δ_{33}
1	TEPO (exp)	49.4	112.5	102.6	−67.0
2	TEPO (QM-Mono)[a]	42.3	112.4	111.6	−97.3
3	TEPO (QM-p)[b]	55.5	112.8	113.9	−65.3
4	TEPO···$B(C_6F_5)_3$ (exp)	75.9	121.7	104.3	1.7
5	TEPO···$B(C_6F_5)_3$ (QM-Mono)[a]	71.3	116.4	103.9	−6.4

[a]NMR values from the monomeric model calculated at the PBE0/pcsSeg-2//ωB97M-D3BJ/def2-TZVPP level of theory. [b]Calculated as a periodic model using the close contacts present in the X-ray crystal structure of TEPO at the PBE/650 eV//PBE0-rVV10/DZVP-MOLOPT-SR-GTH level of theory.

summarizes experimental and calculated ^{31}P NMR tensor data for these compounds. The isotropic chemical shift of free TEPO is 49.4 ppm, which is flanked by spinning sidebands that appear at integer multiples of the rotor spinning frequency (ν_{rot} = 3 kHz). The intensities of the spinning sidebands relate to the δ_{ii} values from the chemical shift tensor in eq 4. Simulation of the experimental spectrum is also shown in Figure 5a and gives (δ_{11}, δ_{22}, δ_{33}) = (112.5, 102.6, −67.0). Similar tensor values were reported previously.[40] At the PBE0/pcsSeg-2//ωB97M-D3BJ/def2-TZVPP level of theory TEPO has predicted NMR parameters with an isotropic chemical shift of 42.3 ppm and (δ_{11}, δ_{22}, δ_{33}) = (112.4, 111.6, −97.3). These values are referenced to ^{31}P NMR chemical shifts for a variety of phosphines and phosphine oxides calculated at the same level of theory (Figure S3.1). The discrepancy in δ_{33} values between theory and experiment is related to the differences in monomeric TEPO, used in the calculation, and the chemical environment encountered in the crystal used for the experimental solid-state NMR measurement. Indeed, the X-ray crystal structure of TEPO shows that each P═O has close contacts to three C−H bonds from a neighboring TEPO.[41] Modeling the chemical shift of a periodic model using the coordinates from the experimental structure at the PBE/650 eV//PBE0-rVV10/DZVP-MOLOPT-SR-GTH level of theory, using a crystal structure optimized with nonlocal dispersion corrections, predicts an isotropic chemical shift of 55.5 ppm and (δ_{11}, δ_{22}, δ_{33}) = (112.8, 113.9, −65.3) that more accurately reproduces the δ_{33} value. These values were referenced to ^{31}P NMR chemical shifts of PPh_3 molecular crystal (Table S1.1).

Figure 5b shows solid-state $^{31}P\{^{1}H\}$ NMR data for TEPO··· $B(C_6F_5)_3$. The isotropic chemical shift is 75.9 ppm, corresponding to a $\Delta\delta$ of 26.5 ppm, close to the $\Delta\delta$ obtained in CD_2Cl_2 solution (26.6 ppm).[42] The simulated spectrum gives (δ_{11}, δ_{22}, δ_{33}) = (121.7, 104.3, 1.7). DFT calculations at the PBE0/pcsSeg-2//ωB97M-D3BJ/def2-TZVPP level of theory predicts $\Delta\delta$ of 29.0 ppm and (δ_{11}, δ_{22}, δ_{33}) = (116.4, 103.9, −6.4), close to experimental values. These data show that δ_{11} and δ_{33} increase with respect to the calculated values for free monomeric TEPO, with δ_{33} shifting far more dramatically than δ_{11}.

Calculated NMR tensor parameters for the complete selection of Lewis acids in Figure 1 are given in Table S7.1. These values were calculated as the difference in shielding constants between free TEPO and the TEPO···Lewis acid adduct These calculated $\Delta\delta_{iso}$ generally agree well with available experimental data. There is no correlation between $\Delta\delta_{iso}$ versus ΔE_{bind} of adduct formation.[17,43] In all adducts studied here, $\Delta\delta_{33}$ shifts to significantly more deshielded values than $\Delta\delta_{11}$ or $\Delta\delta_{22}$. Figure 6a contains simulated static ^{31}P NMR tensors for selected Lewis acids to illustrate this trend.

A plot of $\Delta\delta_{33}$ versus $\Delta\delta_{iso}$ is linear (Figure 6b, R^2 = 0.82), showing that this term in the chemical shift tensor correlates with the isotropic chemical shift. Plots of $\Delta\delta_{11}$ or $\Delta\delta_{22}$ versus $\Delta\delta_{iso}$ correlate poorly (Figure S5.1a–b). This is somewhat unusual because the most deshielded δ_{11} component of the chemical shift tensor is often responsible for downfield NMR chemical shifts.[23b,44,45,46] Plots of $\Delta\delta_{11}$ or $\Delta\delta_{22}$ versus $\Delta E^{(del)}_{O\rightarrow\{P,C\}}$ energies are not linear (Figure S5.3a,b). A plot of $\Delta\delta_{33}$ versus the $\Delta E^{(del)}_{O\rightarrow\{P,C\}}$ is linear (Figure 6c, R^2 = 0.893), indicating that these parameters are related.

The unreferenced chemical shielding tensor shown in eq 4 can be decomposed into a diamagnetic term (σ^d), a result of the effect of $\mathbf{B_0}$ on the ground-state wavefunction of the nucleus, and a paramagnetic term (σ^p) that results in deshielding (eq 5).[23a]

$$\sigma = \sigma^{d} + \sigma^{p} \tag{5}$$

Diamagnetic shielding does not correlate with chemical shift (Figure S5.2a). The $\Delta\delta_{33}$ values shown in Figure 6 are related to σ^p (Figure S5.2b).

The magnitude of σ^p is related to the coupling of a ground state wave function (ϕ_0) to an excited state wave function (ϕ_n) through the angular momentum operator ($\hat{L}_{ki}$, where ki = element of the shielding tensor, eq 6).[47]

$$\sigma_{ij}^{para} \propto \frac{\langle\varphi_0|\hat{L}_{ki}|\varphi_n\rangle\left\langle\varphi_n\left|\frac{\hat{L}_{kNj}}{r^3_{kN}}\right|\varphi_0\right\rangle}{\Delta E_{n-0}} \tag{6}$$

The denominator in eq 6 indicates that if ϕ_0 and ϕ_n are close in energy a large σ^p contribution is expected.[23b,48] Thus, eq 6 connects NMR properties to the orientation of the magnetic shielding tensor, and in turn provides information about the electronic structure at phosphorus. The orientation of the

https://doi.org/10.1021/jacs.5c17621
J. Am. Chem. Soc. 2026, 148, 14768−14778

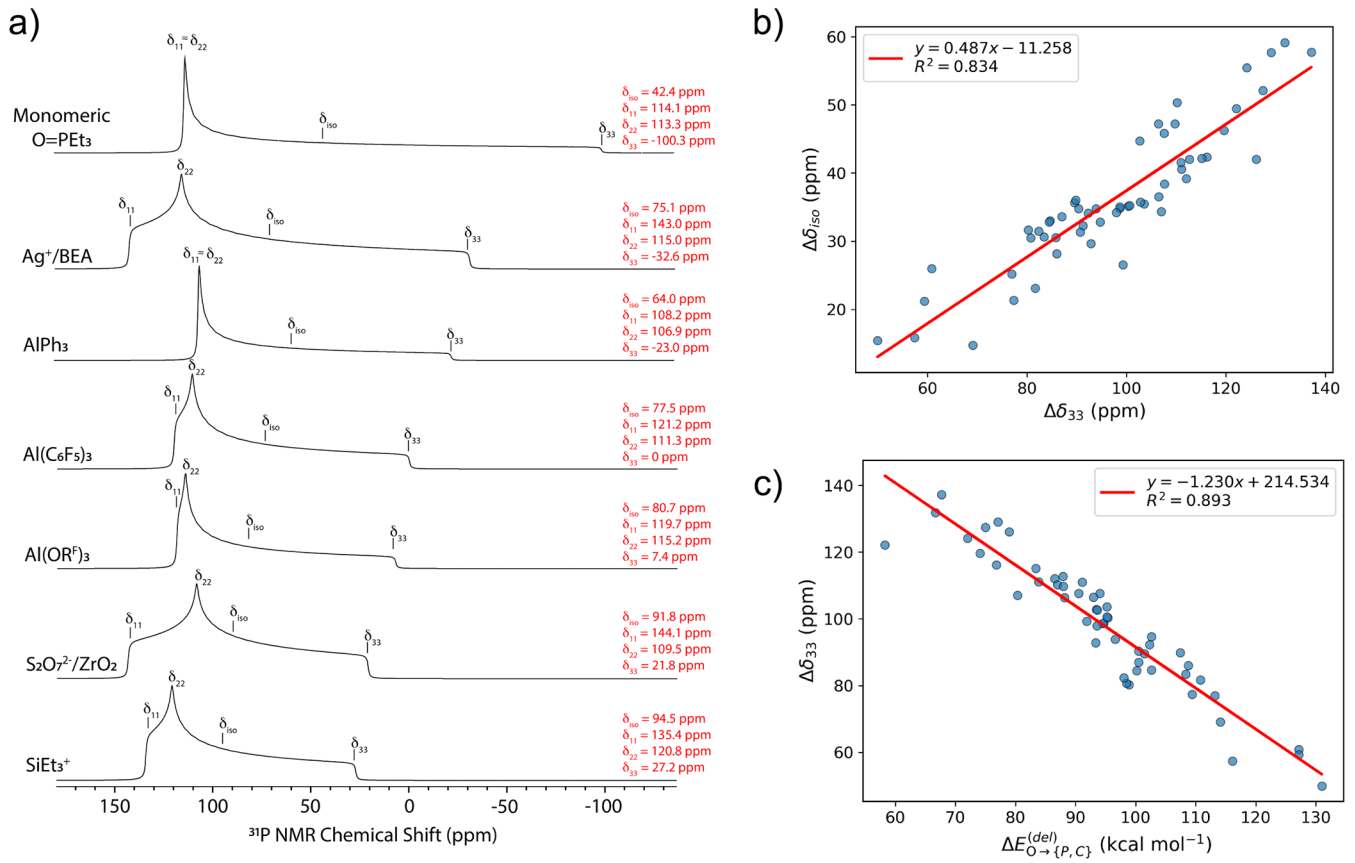

Figure 6. (a) Simulations of the calculated ^{31}P NMR tensors for TEPO adducts of selected Lewis acids. The tensors were simulated using TopSpin 4.4.1 and shown with 250 Hz of line broadening to approximate the static line shape that would be obtained experimentally. The tensor positions for each component (δ_{ii}; i = 1, 2, 3) and isotropic chemical shift (δ_{iso}) are marked in each ^{31}P NMR tensor. The numerical values for each of these components are listed in red. (b) Plot of the change in isotropic chemical shift ($\Delta\delta_{iso}$) and the change in δ_{33} ($\Delta\delta_{33}$). (c) Plot of $\Delta\delta_{33}$ versus $\Delta E^{(del)}_{O\rightarrow\{P,C\}}$ energies showing that weakening of n(O) → σ^*(P−C) hyperconjugation is the primary electronic origin of δ_{33} deshielding.

magnetic shielding tensors for TEPO and TEPO···B$(C_6F_5)_3$ at the ZORA-PBE0/pcSseg-2//ωB97M-D3BJ/def2-TZVPP level of theory are shown in Figure 7. Both tensors are aligned such that σ_{11} and σ_{22} are perpendicular to the P−O bond, while σ_{33} is aligned with the P−O bond. This alignment is conserved across all Lewis adducts.

The origin of (de)shielding was studied using natural chemical shift (NCS) analysis. Quantitative NCS values for NLMO contribution to each shielding term for free TEPO and the Lewis adducts are given in Tables S7.4−S7.6. The qualitative results for free TEPO are shown in Figure 7a. The largest NLMO contributor to paramagnetic deshielding in σ_{11} and σ_{22} is the σ(P−O) orbital. The largest NLMO contributors to σ_{33} are σ(P−C) orbitals. Regardless of the contributor orbital, application of the angular momentum operator results in the formally π^* combination, the LUMO of the molecule. The reason that σ_{11} and σ_{22} are more deshielded than σ_{33} is because the energy gap between σ(P−O) and the π^* is smaller than the energy gap between σ(P−C) and the π^*.

Because the tensors in TEPO and the TEPO···B$(C_6F_5)_3$ are aligned, a similar orbital scheme would be expected. However, NCS analysis shows that σ(P−C) orbitals are the major contributors to paramagnetic deshielding for σ_{11}, σ_{22}, and σ_{33}. In σ_{11} and σ_{22} the angular momentum operator couples the σ(P−C) to σ^*(P−O) orbitals (Figure 7b). This is expected to have a large energy gap and minimal effects on deshielding. The σ(P−O) continues to contribute to σ_{11} and σ_{22}, though less than the σ_{P-C} orbitals. These two effects apparently balance one another and is an explanation of why these two components do not experience significant (de)shielding when TEPO forms an adduct with a Lewis acid.

The orbitals involved in σ_{33} are the same for free TEPO and TEPO···B$(C_6F_5)_3$. The Lewis acid weakens the P═O bond and reduces the energies of the π^* orbitals. This reduces the energy between the σ(P−C) and π^* orbitals, increases σ^p for σ_{33}, results in deshielding of the ^{31}P NMR signal, and is the origin of the relationship between $\Delta\delta_{33}$ and $\Delta E^{(del)}_{O\rightarrow\{P,C\}}$ shown in Figure 6c. These effects are amplified from donation of a second pair of electrons from a different oxygen lone pair into a low-lying σ^* (or empty d_π) orbital. Interactions between Lewis bases and low-lying σ^* orbitals, often referred to as σ-hole interactions, can result in very strong Lewis acids.[49] This breaks π^* degeneracy and reduces the π/π^* energy gap further.

The $\Delta\delta_{iso}$ is the most commonly reported value when assessing Lewis acidity. The correlation between $\Delta\delta_{iso}$ and $\Delta E^{(del)}_{O\rightarrow\{P,C\}}$ energies presented in Figure 8 is rather poor (R^2 = 0.75) compared to the correlation with $\Delta\delta_{33}$ because $\Delta\delta_{11}$ and $\Delta\delta_{22}$ do not systematically increase (or decrease) as a function of P═O bond weakening, which is related to the orbital scheme described in Figure 7. Clearly using only $\Delta\delta_{iso}$ could result in an underestimation of Lewis acidity. This is seen in particular for

https://doi.org/10.1021/jacs.5c17621
J. Am. Chem. Soc. 2026, 148, 14768−14778

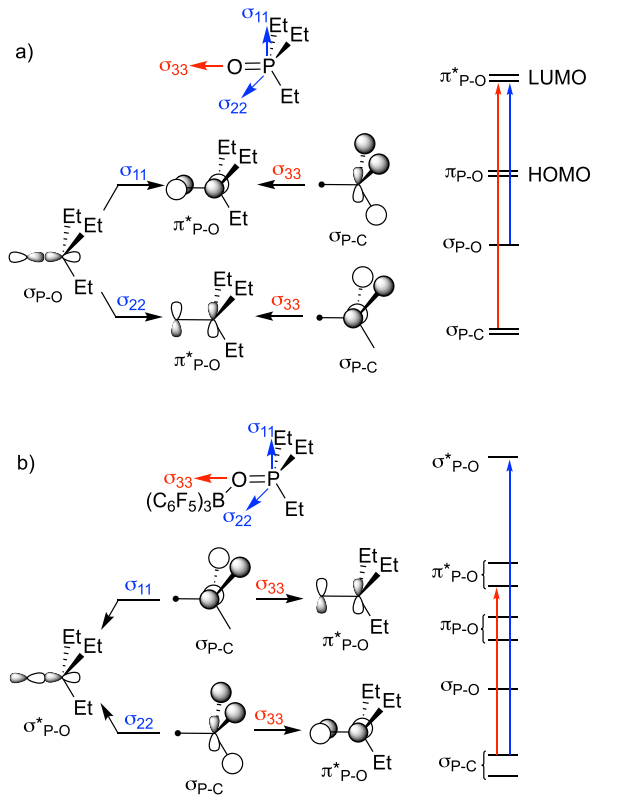

Figure 7. Orientation of the chemical shielding tensors and orbitals involved in σ^{p} deshielding for free TEPO (a) and TEPO···$B(C_6F_5)_3$ (b).

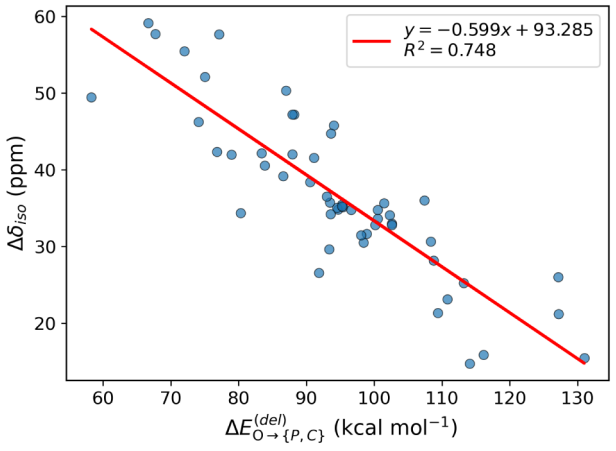

Figure 8. Plot of $\Delta\delta_{iso}$ versus $\Delta E^{(del)}_{O\rightarrow\{P,C\}}$.

$S_2O_7^{2-}/ZrO_2$, which has the lowest $\Delta E^{(del)}_{O\rightarrow\{P,C\}}$ value in the series, but has a low $\Delta\delta_{iso}$ of 49.5 ppm.

The results indicate that arguments about Lewis acidity when using the Gutmann−Beckett method should include solid-state NMR analysis. This is a considerable experimental demand that may not be readily available to many laboratories, and could be further complicated by isolation of potentially unstable species in the solid state. Rubini and coworkers showed that magnetic field dependent T_1 relaxation rates in phosphine oxides and phosphine oxide adducts can deliver some information about the chemical shift tensor in solution.[50] In particular, these measurements give the span (Ω) of the NMR chemical shift tensor, which is the difference between the most shielded and least shielded component of the NMR chemical shift tensor, eq 7:[51]

$$\Omega = \delta_{11} - \delta_{33} \tag{7}$$

In the adducts studied here, Ω generally decreases as Lewis acidity increases, but the correlation between Ω and $\Delta E^{(del)}_{O\rightarrow\{P,C\}}$ is weak (R^2 = 0.67, Figure S5.3c). This is also due to $\Delta\delta_{11}$ and $\Delta\delta_{22}$ that do not systematically increase (or decrease) as a function of P═O bond weakening. This issue can be corrected by approximating δ_{33} using eq 8:

$$\delta_{33} = \frac{3\delta_{iso} - \delta_{22} - \Omega}{2} \tag{8}$$

Though δ_{22} is unknown, the calculated $\Delta\delta_{22}$ values are generally small (Table S7.1). A plot of δ_{33}, calculated using eq 8 but ignoring δ_{22} (i.e., δ_{22} = 0) is shown in Figure 9. Though

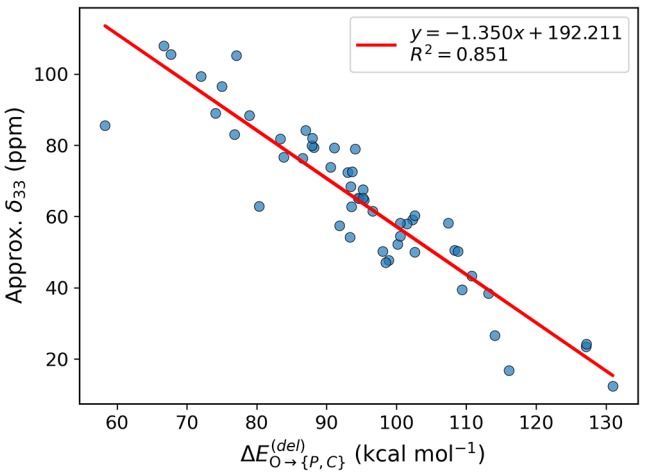

Figure 9. Plot of the approximate δ_{33} calculated with (8) versus $\Delta E^{(del)}_{O\rightarrow\{P,C\}}$.

individual δ_{33} are obviously inaccurate, the correlation implies that approximate $\Delta E^{(del)}_{O\rightarrow\{P,C\}}$ values can be obtained directly from solution $^{31}P\{^1H\}$ NMR measurements, provided T_1 measurements are acquired at multiple magnetic field strengths.

Figure 6c and Figure 9 connect experimental observables, obtained either from solid-state or solution $^{31}P\{^1H\}$ NMR measurements, to $\Delta E^{(del)}_{O\rightarrow\{P,C\}}$ obtained from quantum chemical calculations. While $\Delta E^{(del)}_{O\rightarrow\{P,C\}}$ is an abstract value derived within the NBO formalism, its "real-world" meaning is straightforward: $\Delta E^{(del)}_{O\rightarrow\{P,C\}}$ represents the decrease of P═O bond delocalization and the degree to which the Lewis acid has weakened the P═O bond. In this sense, $\Delta\delta_{33}$ can be understood as an experimental spectroscopic approximation of the intrinsic P═O bond strength, with both quantities independently tracking the same underlying electronic consequences. Thus, one practical outcome of this study is that DFT-calculated energies are not strictly necessary to assess Lewis acid strength via the Gutmann−Beckett method—the ^{31}P NMR chemical shift tensor, and in particular $\Delta\delta_{33}$ component, provides direct experimental access to the same information. This statement comes with the caveat that TEPO must bind sufficiently strongly to form a stable adduct and that measurements must be conducted in the absence of exchange dynamics.

https://doi.org/10.1021/jacs.5c17621
J. Am. Chem. Soc. 2026, 148, 14768−14778

CONCLUSION

The experimentalist should exercise caution when using the Gutmann−Beckett method. This study shows that there are correlations between ^{31}P NMR properties and P═O bond weakening, which is a thermodynamic descriptor of Lewis acid strength, but the correlation between the most commonly reported change in isotropic ^{31}P NMR chemical shift ($\Delta\delta_{iso}$) and P═O bond strength is weak. Two solutions are proposed. Acquisition of solid-state ^{31}P{^{1}H} NMR data to extract $\Delta\delta_{33}$ values that are correlated well with P═O bond weakening. In the absence of these measurements, solution T_1 measurements at multiple field strengths allows the user to approximate $\Delta E^{(del)}_{O\rightarrow\{P,C\}}$ from the linear regression shown in Figure 9.

The reason for this behavior is that only the most shielded δ_{33} component of the ^{31}P NMR chemical shift tensor is dramatically affected in TEPO adducts, and the changes in δ_{33} track with overall change in ^{31}P NMR chemical shift far better than the more deshielded δ_{11} or δ_{22} components. NCS analysis shows that this is due to $\Delta\delta_{33}$ coupling filled P−C bonding orbitals to empty π^* orbitals. Bond weakening narrows the π/π^* HOMO−LUMO gap, which results in more paramagnetic deshielding as stronger Lewis acids further weaken the P═O bond.

This trend holds across a chemically diverse set of molecular Lewis acids and small cluster models that approximate Lewis sites on heterogeneous surfaces. The latter case is particularly valuable for those who study heterogeneous catalysts because Lewis sites play a significant role in activating substrates on these materials and their molecular structure is often difficult to assess or compare to small molecules.

Finally, Lewis acid strength is a nebulous parameter. Brønsted (H^+) acidity is described by straightforward thermodynamic descriptors (e.g., pK_a, deprotonation energy (DPE), etc.) because the proton does not need to structurally adapt to a base in the way that a Lewis acid must. This is part of the reason why so many of the useful scales that measure Lewis acidity (^{19}F NMR,[52] Fluoride ion affinity,[53] Hydride ion affinity,[54] Global electrophilicity index,[55] etc.) usually do not correlate with one another. We do not propose a solution to this challenge, but hope that this study shows that the Gutmann−Beckett method, if viewed in more granular detail than just $\Delta\delta_{iso}$, has validity because P═O bond weakening is a thermodynamic descriptor of Lewis acid strength.

ASSOCIATED CONTENT

Data Availability Statement

All underlying data sets presented and discussed in this study are available via 4TU.ResearchData at DOI: https://doi.org/10.4121/426e8bc2-27a5-4eb6-8fec-541c02733dd5.

Supporting Information

The Supporting Information is available free of charge at https://pubs.acs.org/doi/10.1021/jacs.5c17621.

The geometries of the models under consideration (ZIP)

Raw data (CSV)

List of models, computational and experimental details, analysis of the principal components of the chemical shielding (PDF)

AUTHOR INFORMATION

Corresponding Authors

Matthew P. Conley − *Department of Chemistry, University of California, Riverside, California 92507, United States;* orcid.org/0000-0001-8593-5814; Email: matthew.conley@ucr.edu

Evgeny A. Pidko − *Inorganic Systems Engineering Group, Department of Chemical Engineering, Faculty of Applied Sciences, Delft University of Technology, Delft 2629 HZ, The Netherlands;* orcid.org/0000-0001-9242-9901; Email: e.a.pidko@tudelft.nl

Authors

Alexander A. Kolganov − *Inorganic Systems Engineering Group, Department of Chemical Engineering, Faculty of Applied Sciences, Delft University of Technology, Delft 2629 HZ, The Netherlands;* orcid.org/0000-0002-0262-8892

Maximillian Kling − *Department of Chemistry, University of California, Riverside, California 92507, United States;* orcid.org/0009-0006-8792-1030

Complete contact information is available at: https://pubs.acs.org/10.1021/jacs.5c17621

Notes

The authors declare no competing financial interest.

ACKNOWLEDGMENTS

This research was supported by the National Science Foundation (CHE-2453538, M.P.C.). E.A.P. thanks NWO Domain Science for support in the framework of the DynaCat VICI grant (VI.C.242.082, 10.61686/WNCYG94137). The use of supercomputer facilities was sponsored by NWO Domain Science (2024.008, A.A.K., E.A.P.).

REFERENCES

(1) Atkins, P. *Shriver and Atkins' Inorganic Chemistry*; Oxford University Press, 2010.

(2) Yamamoto, H. *In Lewis Acids in Organic Synthesis*; Wiley-VCH, 2000.

(3) (a) Hounjet, L. J.; Stephan, D. W. Hydrogenation by Frustrated Lewis Pairs: Main Group Alternatives to Transition Metal Catalysts? *Org. Process Res. Dev.* **2014**, *18*, 385−391. (b) Stephan, D. W. Frustrated Lewis Pairs. *J. Am. Chem. Soc.* **2015**, *137*, 10018−10032.

(4) (a) Stephan, D. W. Frustrated Lewis Pairs: From Concept to Catalysis. *Acc. Chem. Res.* **2015**, *48*, 306−316. (b) Meng, W.; Feng, X.; Du, H. Frustrated Lewis Pairs Catalyzed Asymmetric Metal-Free Hydrogenations and Hydrosilylations. *Acc. Chem. Res.* **2018**, *51*, 191−201. (c) Stephan, D. W.; Erker, G. Frustrated Lewis Pairs: Metal-free Hydrogen Activation and More. *Angew. Chem., Int. Ed.* **2010**, *49*, 46−76.

(5) (a) Corma, A.; García, H. Lewis Acids: From Conventional Homogeneous to Green Homogeneous and Heterogeneous Catalysis. *Chem. Rev.* **2003**, *103*, 4307−4366. (b) Román-Leshkov, Y.; Davis, M. E. Activation of Carbonyl-Containing Molecules with Solid Lewis Acids in Aqueous Media. *ACS Catal.* **2011**, *1*, 1566−1580. (c) Li, J.; Li, G.; Tsang, S. C. E. Heterogeneous Frustrated Lewis Pair Catalysts: Rational Structure Design and Mechanistic Elucidation Based on Intrinsic Properties of Supports. *Acc. Chem. Res.* **2025**, *58*, 555−569. (d) Liu, K.; Liu, T.; Wu, X.; Jiao, X.; Du, P.; Wan, J.; Heine, T.; Liu, L. Structures and reactivities of heterogeneous frustrated Lewis pairs catalysts. *Coord. Chem. Rev.* **2026**, *546*, 217039.

(6) (a) Khivantsev, K.; Jaegers, N. R.; Kwak, J.-H.; Szanyi, J.; Kovarik, L. Precise Identification and Characterization of Catalytically Active Sites on the Surface of γ-Alumina. *Angew. Chem., Int. Ed.* **2021**, *60*,

17522−17530. (b) Wischert, R.; Copéret, C.; Delbecq, F.; Sautet, P. Optimal Water Coverage on Alumina: A Key to Generate Lewis Acid−Base Pairs that are Reactive Towards the C−H Bond Activation of Methane. *Angew. Chem., Int. Ed.* **2011**, *50*, 3202−3205. (c) Wischert, R.; Laurent, P.; Copéret, C.; Delbecq, F.; Sautet, P. A. The Essential and Unexpected Role of Water for the Structure, Stability, and Reactivity of 'Defect. *Sites. J. Am. Chem. Soc.* **2012**, *134*, 14430−14449. (d) Valla, M.; Wischert, R.; Comas-Vives, A.; Conley, M. P.; Verel, R.; Copéret, C.; Sautet, P. Role of Tricoordinate Al Sites in CH_3ReO_3/Al_2O_3 Olefin Metathesis Catalysts. *J. Am. Chem. Soc.* **2016**, *138*, 6774−6785. (e) Motta, A.; Fragalà, I. L.; Marks, T. J. Links Between Single-Site Heterogeneous and Homogeneous Catalysis. DFT Analysis of Pathways for Organozirconium Catalyst Chemisorptive Activation and Olefin Polymerization on γ-Alumina. *J. Am. Chem. Soc.* **2008**, *130*, 16533−16546.

(7) (a) Marks, T. J. Surface-bound metal hydrocarbyls. Organometallic connections between heterogeneous and homogeneous catalysis. *Acc. Chem. Res.* **1992**, *25* (25), 57−65. (b) Toscano, P. J.; Marks, T. J. Supported organoactinides. High-resolution solid-state carbon-13 NMR studies of catalytically active, alumina-bound pentamethylcyclopentadienyl)thorium methyl and hydride complexes. *J. Am. Chem. Soc.* **1985**, *107*, 653−659. (c) Joubert, J.; Delbecq, F.; Sautet, P.; Roux, E. L.; Taoufik, M.; Thieuleux, C.; Blanc, F.; Copéret, C.; Thivolle-Cazat, J.; Basset, J.-M. Molecular Understanding of Alumina Supported Single-Site Catalysts by a Combination of Experiment and Theory. *J. Am. Chem. Soc.* **2006**, *128*, 9157−9169. (d) Culver, D. B.; Dorn, R. W.; Venkatesh, A.; Meeprasert, J.; Rossini, A. J.; Pidko, E. A.; Lipton, A. S.; Lief, G. R.; Conley, M. P. Active Sites in a Heterogeneous Organometallic Catalyst for the Polymerization of Ethylene. *ACS Cent. Sci.* **2021**, *7*, 1225−1231.

(8) (a) Ahrens, M.; Scholz, G.; Braun, T.; Kemnitz, E. Catalytic Hydrodefluorination of Fluoromethanes at Room Temperature by Silylium-ion-like Surface Species. *Angew. Chem., Int. Ed.* **2013**, *52*, 5328−5332. (b) Kemnitz, E.; Gross, U.; Rudiger, S.; Shekar, C. S. Amorphous metal fluorides with extraordinary high surface areas. *Angew. Chem., Int. Ed.* **2003**, *42*, 4251−4254. (c) Krahl, T.; Kemnitz, E. Aluminium fluoride - the strongest solid Lewis acid: structure and reactivity. *Catal. Sci. Technol.* **2017**, *7*, 773−796.

(9) (a) Culver, D. B.; Conley, M. P. Activation of C−F Bonds by Electrophilic Organosilicon Sites Supported on Sulfated Zirconia. *Angew. Chem., Int. Ed.* **2018**, *57*, 14902−14905. (b) Culver, D. B.; Venkatesh, A.; Huynh, W.; Rossini, A. J.; Conley, M. P. $Al(OR^F)_3$ (R^F = $C(CF_3)_3$) activated silica: a well-defined weakly coordinating surface anion. *Chem. Sci.* **2020**, *11*, 1510−1517. (c) Samudrala, K. K.; Conley, M. P. Effects of surface acidity on the structure of organometallics supported on oxide surfaces. *Chem. Commun.* **2023**, *59*, 4115−4127.

(10) Li, G.; Pidko, E. A. The Nature and Catalytic Function of Cation Sites in Zeolites: a Computational Perspective. *ChemCatchem* **2019**, *11*, 134−156.

(11) (a) Copéret, C. Single-Sites and Nanoparticles at Tailored Interfaces Prepared via Surface Organometallic Chemistry from Thermolytic Molecular Precursors. *Acc. Chem. Res.* **2019**, *52*, 1697−1708. (b) Fujdala, K. L.; Brutchey, R. L.; Tilley, T. D.Tailored Oxide Materials via Thermolytic Molecular Precursor (TMP) Methods*Surface and Interfacial Organometallic Chemistry and Catalysis*SpringerBerlin, Heidelberg200569−115

(12) (a) Kazansky, V. B.; Pidko, E. A. Intensities of IR Stretching Bands as a Criterion of Polarization and Initial Chemical Activation of Adsorbed Molecules in Acid Catalysis. Ethane Adsorption and Dehydrogenation by Zinc Ions in ZnZSM-5 Zeolite. *J. Phys. Chem. B* **2005**, *109*, 2103−2108. (b) Kolganov, A. A.; Gabrienko, A. A.; Chernyshov, I. Y.; Stepanov, A. G.; Pidko, E. A. Property−activity relations of multifunctional reactive ensembles in cation-exchanged zeolites: a case study of methane activation on Zn^{2+} modified zeolite BEA. *Phys. Chem. Chem. Phys.* **2022**, *24*, 6492−6504. (c) Conley, M. P.; Delley, M. F.; Nunez-Zarur, F.; Comas-Vives, A.; Copéret, C. Heterolytic Activation of C−H Bonds on Cr(III)−O Surface Sites Is a Key Step in Catalytic Polymerization of Ethylene and Dehydrogenation of Propane. *Inorg. Chem.* **2015**, *54*, 5065−5073.

(13) (a) Sattler, J. J. H. B.; Ruiz-Martinez, J.; Santillan-Jimenez, E.; Weckhuysen, B. M. Catalytic Dehydrogenation of Light Alkanes on Metals and Metal Oxides. *Chem. Rev.* **2014**, *114*, 10613−10653. (b) Schweitzer, N. M.; Hu, B.; Das, U.; Kim, H.; Greeley, J.; Curtiss, L. A.; Stair, P. C.; Miller, J. T.; Hock, A. S. Propylene Hydrogenation and Propane Dehydrogenation by a Single-Site Zn^{2+} on Silica Catalyst. *ACS Catal.* **2014**, *4*, 1091−1098. (c) Hu, B.; Getsoian, A. B.; Schweitzer, N. M.; Das, U.; Kim, H.; Niklas, J.; Poluektov, O.; Curtiss, L. A.; Stair, P. C.; Miller, J. T.; et al. Selective propane dehydrogenation with single-site CoII on SiO2 by a non-redox mechanism. *J. Catal.* **2015**, *322*, 24−37. (d) Searles, K.; Siddiqi, G.; Safonova, O. V.; Copéret, C. Silica-supported isolated gallium sites as highly active, selective and stable propane dehydrogenation catalysts. *Chem. Sci.* **2017**, *8*, 2661−2666.

(14) (a) Conley, M. P.; Delley, M. F.; Siddiqi, G.; Lapadula, G.; Norsic, S.; Monteil, V.; Safonova, O. V.; Copéret, C. Polymerization of Ethylene by Silica-Supported Dinuclear Cr(III) Sites through an Initiation Step Involving C-H Bond Activation. *Angew. Chem., Int. Ed.* **2014**, *53*, 1872−1876. (b) Delley, M. F.; Nunez-Zarur, F.; Conley, M. P.; Comas-Vives, A.; Siddiqi, G.; Norsic, S.; Monteil, V.; Safonova, O. V.; Copéret, C. Proton transfers are key elementary steps in ethylene polymerization on isolated chromium(III) silicates. *Proc. Natl. Acad. Sci. U.S.A.* **2014**, *111*, 11624−11629. (c) Delley, M. F.; Lapadula, G.; Núñez-Zarur, F.; Comas-Vives, A.; Kalendra, V.; Jeschke, G.; Baabe, D.; Walter, M. D.; Rossini, A. J.; Lesage, A.; Emsley, L.; Maury, O.; Copéret, C. Local Structures and Heterogeneity of Silica-Supported M(III) Sites Evidenced by EPR, IR, NMR, and Luminescence Spectroscopies. *J. Am. Chem. Soc.* **2017**, *139*, 8855−8867.

(15) *Lewis acidity: IUPAC Compendium of Chemical Terminology*, 5.0.0th ed.; International Union of Pure and Applied Chemistry (IUPAC), 2025.

(16) (a) Beckett, M. A.; Strickland, G. C.; Holland, J. R.; Sukumar Varma, K. A convenient n.m.r. method for the measurement of Lewis acidity at boron centres: correlation of reaction rates of Lewis acid initiated epoxide polymerizations with Lewis acidity. *Polymer* **1996**, *37*, 4629−4631. (b) Mayer, U.; Gutmann, V.; Gerger, W. The acceptor number — A quantitative empirical parameter for the electrophilic properties of solvents. *Monats. für Chem.* **1975**, *106*, 1235−1257.

(17) Erdmann, P.; Greb, L. What Distinguishes the Strength and the Effect of a Lewis Acid: Analysis of the Gutmann−Beckett Method. *Angew. Chem., Int. Ed.* **2022**, *61*, No. e202114550.

(18) Golwankar, R. R.; Curry, T. D., II; Paranjothi, C. J.; Blakemore, J. D. Molecular Influences on the Quantification of Lewis Acidity with Phosphine Oxide Probes. *Inorg. Chem.* **2023**, *62*, 9765−9780.

(19) (a) Yi, X.; Ko, H.-H.; Deng, F.; Liu, S.-B.; Zheng, A. Solid-state ^{31}P NMR mapping of active centers and relevant spatial correlations in solid acid catalysts. *Nat. Protoc.* **2020**, *15*, 3527−3555. (b) Gabrienko, A. A.; Chaemchuen, S.; Kou, Z.; Ogiwara, N.; Kitagawa, H.; Khudozhitkov, A. E.; Stepanov, A. G.; Kolokolov, D. I.; Verpoort, F. The Nature of Structural Defects in ZIF-8 Revealed with ^{1}H and ^{31}P MAS NMR and X-Ray Absorption Spectroscopy. *Angew. Chem. Int. Ed.* **2025**, *64*, No. e202414823. (c) Zheng, A.; Liu, S.-B.; Deng, F. ^{31}P NMR Chemical Shifts of Phosphorus Probes as Reliable and Practical Acidity Scales for Solid and Liquid Catalysts. *Chem. Rev.* **2017**, *117*, 12475−12531.

(20) However, sterically small phosphine oxides can adsorb on Brønsted sites to form dimeric adducts, see: Bornes, C.; Fischer, M.; Amelse, J. A.; Geraldes, C. F.; Rocha, J.; Mafra, L. What Is Being Measured with P-Bearing NMR Probe Molecules Adsorbed on Zeolites? *J. Am. Chem. Soc.* **2021**, *143*, 13616−13623.

(21) (a) Osegovic, J. P.; Drago, R. S. Measurement of the Global Acidity of Solid Acids by ^{31}P MAS NMR of Chemisorbed Triethylphosphine Oxide. *J. Phys. Chem. B* **2000**, *104*, 147−154. (b) Zheng, A.; Zhang, H.; Lu, X.; Liu, S.-B.; Deng, F. Theoretical Predictions of ^{31}P NMR Chemical Shift Threshold of Trimethylphosphine Oxide Absorbed on Solid Acid Catalysts. *J. Phys. Chem. B* **2008**, *112*, 4496−4505.

(22) Reed, C. A. Myths about the Proton. The Nature of H^+ in Condensed Media. *Acc. Chem. Res.* **2013**, *46*, 2567−2575.

https://doi.org/10.1021/jacs.5c17621
J. Am. Chem. Soc. 2026, 148, 14768−14778

(23) (a) Widdifield, C. M.; Schurko, R. W. Understanding chemical shielding tensors using group theory, MO analysis, and modern density-functional theory. *Conc. Mag. Res. A* **2009**, *34A*, 91−123. (b) Gordon, C. P.; Raynaud, C.; Andersen, R. A.; Copéret, C.; Eisenstein, O. Carbon-13 NMR Chemical Shift: A Descriptor for Electronic Structure and Reactivity of Organometallic Compounds. *Acc. Chem. Res.* **2019**, *52*, 2278−2289.
(24) Müller, L. O.; Himmel, D.; Stauffer, J.; Steinfeld, G.; Slattery, J.; Santiso-Quiñones, G.; Brecht, V.; Krossing, I. Simple Access to the Non-Oxidizing Lewis Superacid $PhF{\rightarrow}Al(OR^F)_3$ ($R^F = C(CF_3)_3$). *Angew. Chem., Int. Ed.* **2008**, *47*, 7659−7663.
(25) Akram, M. O.; Tidwell, J. R.; Dutton, J. L.; Martin, C. D. *Tris*(ortho-carboranyl)borane: An Isolable, Halogen-Free, Lewis Superacid. *Angew. Chem., Int. Ed.* **2022**, *134*, No. e202212073.
(26) Akram, M. O.; Tidwell, J. R.; Dutton, J. L.; Martin, C. D. *Bis*(1-Methyl-ortho-Carboranyl)Borane. *Angew. Chem., Int. Ed.* **2023**, *62*, No. e202307040.
(27) Shoji, Y.; Tanaka, N.; Mikami, K.; Uchiyama, M.; Fukushima, T. A two-coordinate boron cation featuring $C{-}B^{+}{-}C$ bonding. *Nat. Chem.* **2014**, *6*, 498−503.
(28) Pan, B.; Gabbaï, F. P. $[Sb(C_6F_5)_4][B(C_6F_5)_4]$: An Air Stable, Lewis Acidic Stibonium Salt That Activates Strong Element-Fluorine Bonds. *J. Am. Chem. Soc.* **2014**, *136*, 9564−9567.
(29) Samudrala, K. K.; Huynh, W.; Dorn, R. W.; Rossini, A. J.; Conley, M. P. Formation of a Strong Heterogeneous Aluminum Lewis Acid on Silica. *Angew. Chem., Int. Ed.* **2022**, *61*, No. e202205745.
(30) Samudrala, K. K.; Akram, M. O.; Dutton, J. L.; Martin, C. D.; Conley, M. P. Formation of Strong Boron Lewis Acid Sites on Silica. *Inorg. Chem.* **2024**, *63*, 4939−4946.
(31) Jammee, R.; Kolganov, A.; Groves, M. C.; Pidko, E. A.; Sydora, O. L.; Conley, M. P. C−H Bond Activation by Sulfated Zirconium Oxide is Mediated by a Sulfur-Centered Lewis Superacid. *Angew. Chem., Int. Ed.* **2025**, *64*, No. e202421699.
(32) Kolganov, A. A.; Gabrienko, A. A.; Stepanov, A. G. The DFT Approach to predict ^{13}C NMR chemical shifts of hydrocarbon species adsorbed on Zn-modified zeolites. *Phys. Chem. Chem. Phys.* **2022**, *24*, 22241−22249.
(33) Reed, A. E.; Weinhold, F. Natural localized molecular orbitals. *J. Chem. Phys.* **1985**, *83*, 1736−1740.
(34) (a) Glendening, E. D.; Badenhoop, J. K.; Reed, A. E.; Carpenter, J. E.; Bohmann, J. A.; Morales, C. M.; Karafiloglou, P.; Landis, C. R.; Weinhold, F. *NBO 7.0. Theoretical Chemistry Institute*; University of Wisconsin, Madison, 2018. (b) Glendening, E. D.; Landis, C. R.; Weinhold, F. NBO 7.0: New vistas in localized and delocalized chemical bonding theory. *J. Comput. Chem.* **2019**, *40*, 2234−2241.
(35) (a) Chesnut, D. B. An Ab Initio Nuclear Magnetic Resonance and Atoms-in-Molecules Study of the PO Bond in Phosphine Oxides. *J. Am. Chem. Soc.* **1998**, *120*, 10504−10510. (b) Chesnut, D. B.; Savin, A. The Electron Localization Function (ELF) Description of the PO Bond in Phosphine Oxide. *J. Am. Chem. Soc.* **1999**, *121*, 2335−2336. (c) Gilheany, D. G. No d Orbitals but Walsh Diagrams and Maybe Banana Bonds: Chemical Bonding in Phosphines Phosphine Oxides, and Phosphonium Ylides. *Chem. Rev.* **1994**, *94*, 1339−1374. (d) Reed, A. E.; Schleyer, P. V. R. Chemical bonding in hypervalent molecules. The dominance of ionic bonding and negative hyperconjugation over d-orbital participation. *J. Am. Chem. Soc.* **1990**, *112*, 1434−1445.
(36) Yamada, K.; Koga, N. Variationally determined electronic states for the theoretical analysis of intramolecular interaction. II. Qualitative nature of the P = O bond in phosphine oxides. *J. Comput. Chem.* **2013**, *34*, 149−161.
(37) Beckett, M. A.; Brassington, D. S.; Coles, S. J.; Hursthouse, M. B. Lewis acidity of tris(pentafluorophenyl)borane: crystal and molecular structure of $B(C_6F_5)_3{\cdot}OPEt_3$. *Inorg. Chem. Commun.* **2000**, *3*, 530−533.
(38) Glendening, E. D.; Landis, C. R.; Weinhold, F. NBO 6.0: Natural bond orbital analysis program. *J. Comput. Chem.* **2013**, *34*, 1429−1437.
(39) (a) Ma, C. T. L.; MacLachlan, M. J. Supramolecular Assembly and Coordination-Assisted Deaggregation of Multimetallic Macrocycles. *Angew. Chem., Int. Ed.* **2005**, *44*, 4178−4182. (b) Kleij, A. W. Zinc-centred salen complexes: versatile and accessible supramolecular building motifs. *Dalton Trans.* **2009**, 4635−4639.
(40) (a) Robert, J. B.; Wiesenfeld, L. ^{31}P solid state nuclear magnetic resonance principal values of the chemical shift tensors of phosphane oxides, phosphane sulphides and phosphane selenides. *Mol. Phys.* **1981**, *44*, 319−327. (b) Shenderovich, I. G. Effect of Noncovalent Interactions on the ^{31}P Chemical Shift Tensor of Phosphine Oxides, Phosphinic, Phosphonic, and Phosphoric Acids, and Their Complexes with Lead(II). *J. Phys. Chem. C* **2013**, *117*, 26689−26702.
(41) Bolte, M. *Cambridge Crystallographic Data Centre*, 2025.
(42) Morgan, M. M.; Marwitz, A. J. V.; Piers, W. E.; Parvez, M. Comparative Lewis Acidity in Fluoroarylboranes: $B(o\text{-}HC_6F_4)_3$, $B(p\text{-}HC_6F_4)_3$, and $B(C_6F_5)_3$. *Organometallics* **2013**, *32*, 317−322.
(43) (a) Similar observations were made previously in studies of phosphine oxide adducts of $B(oCb)_3$ and $HB^{Me}oCb_2$, see: Ranasinghe, S.; Li, Y.; Andrews, M. E.; Akram, M. O.; Thornton, R. A.; Martin, C. D. Müller versus Gutmann−Beckett for assessing the Lewis acidity of boranes. *Chem. Commun.* **2025**, *61*, 10182−10185. (b) Akram, M. O.; Martin, C. D.; Dutton, J. L. The Effect of Carborane Substituents on the Lewis Acidity of Boranes. *Inorg Chem.* **2023**, *62*, 13495−13504.
(44) (a) Yang, M.; Tofan, D.; Chen, C.-H.; Jack, K. M.; Gabbaï, F. P. Digging the Sigma-Hole of Organoantimony Lewis Acids by Oxidation. *Angew. Chem., Int. Ed.* **2018**, *57*, 13868−13872. (b) Lim, J. Y. C.; Beer, P. D. Sigma-Hole Interactions in Anion Recognition. *Chem* **2018**, *4*, 731−783. (c) Zhou, B.; Gabbaï, F. P. Redox-controlled chalcogen-bonding at tellurium: impact on Lewis acidity and chloride anion transport properties. *Chem. Sci.* **2020**, *11*, 7495−7500. (d) Murphy, B. L.; Gabbaï, F. P. Tunable Pnictogen Bonding at the Service of Hydroxide Transport across Phospholipid Bilayers. *J. Am. Chem. Soc.* **2024**, *146*, 7146−7151.
(45) (a) Berger, S.; Fleischer, U.; Geletneky, C.; Lohrenz, J. C. W. The ^{13}C Chemical Shift of the ipso Carbon Atom in Phenyllithium. *Chem. Ber.* **1995**, *128*, 1183−1186. (b) Pinter, B.; Smith, K. T.; Kamitani, M.; Zolnhofer, E. M.; Tran, B. L.; Fortier, S.; Pink, M.; Wu, G.; Manor, B. C.; Meyer, K.; Baik, M.-H.; Mindiola, D. J. Cyclo-P_3 Complexes of Vanadium: Redox Properties and Origin of the ^{31}P NMR Chemical Shift. *J. Am. Chem. Soc.* **2015**, *137*, 15247−15261. (c) Autschbach, J.; Zheng, S. Analyzing Pt chemical shifts calculated from relativistic density functional theory using localized orbitals: The role of Pt 5d lone pairs. *Magn. Reson. Chem.* **2008**, *46*, S45−S55. (d) Gordon, C. P.; Yamamoto, K.; Liao, W. C.; Allouche, F.; Andersen, R. A.; Coperet, C.; Raynaud, C.; Eisenstein, O. Metathesis Activity Encoded in the Metallacyclobutane Carbon-13 NMR Chemical Shift Tensors. *ACS Cent. Sci.* **2017**, *3*, 759−768. (e) Yamamoto, K.; Gordon, C. P.; Liao, W. C.; Coperet, C.; Raynaud, C.; Eisenstein, O. Orbital Analysis of Carbon-13 Chemical Shift Tensors Reveals Patterns to Distinguish Fischer and Schrock Carbenes. *Angew. Chem., Int. Ed.* **2017**, *56*, 10127−10131. (f) Gordon, C. P.; Yamamoto, K.; Searles, K.; Shirase, S.; Andersen, R. A.; Eisenstein, O.; Coperet, C. Metal alkyls programmed to generate metal alkylidenes by alpha-H abstraction: prognosis from NMR chemical shift. *Chem. Sci.* **2018**, *9*, 1912−1918. (g) Estes, D. P.; Gordon, C. P.; Fedorov, A.; Liao, W. C.; Ehrhorn, H.; Bittner, C.; Zier, M. L.; Bockfeld, D.; Chan, K. W.; Eisenstein, O.; Raynaud, C.; Tamm, M.; Coperet, C. Molecular and Silica-Supported Molybdenum Alkyne Metathesis Catalysts: Influence of Electronics and Dynamics on Activity Revealed by Kinetics Solid-State NMR, and Chemical Shift Analysis. *J. Am. Chem. Soc.* **2017**, *139*, 17597−17607. (h) Halbert, S.; Coperet, C.; Raynaud, C.; Eisenstein, O. Elucidating the Link between NMR Chemical Shifts and Electronic Structure in d(0) Olefin Metathesis Catalysts. *J. Am. Chem. Soc.* **2016**, *138*, 2261−2272. (i) Culver, D. B.; Huynh, W.; Tafazolian, H.; Ong, T.-C.; Conley, M. P. The β-Agostic Structure in $(C_5Me_5)_2Sc(CH_2CH_3)$: Solid-State NMR Studies of $(C_5Me_5)_2Sc{-}R$ (R = Me, Ph, Et). *Angew. Chem., Int. Ed.* **2018**, *57*, 9520−9523. (j) Gordon, C. P.; Copéret, C. Metal Alkyls with Alkylidynic Metal-Carbon Bond Character: Key Electronic Structures in Alkane Metathesis Precatalysts. *Angew. Chem., Int. Ed.* **2020**, *59*, 7035−7041. (k) Wu, G.; Rovnyak, D.; Johnson, M. J. A.; Zanetti, N. C.; Musaev, D. G.; Morokuma, K.; Schrock, R. R.; Griffin, R. G.; Cummins, C. C. Unusual ^{31}P Chemical Shielding Tensors in Terminal Phosphido

https://doi.org/10.1021/jacs.5c17621
J. Am. Chem. Soc. 2026, 148, 14768−14778

Complexes Containing a Phosphorus−Metal Triple Bond. *J. Am. Chem. Soc.* **1996**, *118*, 10654−10655. (l) Huynh, W.; Conley, M. P. Origin of the ^{29}Si NMR chemical shift in R_3Si-X and relationship to the formation of silylium (R_3Si^+) ions. *Dalton Trans.* **2020**, *49*, 16453−16463.

(46) The carbonyl signal in peptides experience deshielding of δ_{22} when engaged in hydrogen bonding, see: Gu, Z.; Zambrano, R.; McDermott, A. Hydrogen bonding of carboxyl groups in solid-state amino acids and peptides: comparison of carbon chemical shielding, infrared frequencies, and structures. *J. Am. Chem. Soc.* **1994**, *116*, 6368−6372.

(47) (a) Ramsey, N. F. Electron Coupled Interactions between Nuclear Spins in Molecules. *Phys. Rev.* **1953**, *91*, 303−307. (b) Ramsey, N. F. Magnetic Shielding of Nuclei in Molecules. *Phys. Rev.* **1950**, *78*, 699−703.

(48) (a) Facelli, J. C. Chemical shift tensors: Theory and application to molecular structural problems. *Prog. Nucl. Magn. Reson. Spectrosc.* **2011**, *58*, 176−201. (b) Autschbach, J. Analyzing NMR shielding tensors calculated with two-component relativistic methods using spin-free localized molecular orbitals. *J. Chem. Phys.* **2008**, *128*, 164112.

(49) (a) Yang, M.; Tofan, D.; Chen, C.-H.; Jack, K. M.; Gabbaï, F. P. Digging the Sigma-Hole of Organoantimony Lewis Acids by Oxidation. *Angew. Chem., Int. Ed.* **2018**, *57*, 13868−13872. (b) Lim, J. Y. C.; Beer, P. D. Sigma-Hole Interactions in Anion Recognition. *Chem* **2018**, *4*, 731−783. (c) Zhou, B.; Gabbaï, F. P. Redox-controlled chalcogen-bonding at tellurium: impact on Lewis acidity and chloride anion transport properties. *Chem. Sci.* **2020**, *11*, 7495−7500. (d) Murphy, B. L.; Gabbaï, F. P. Tunable Pnictogen Bonding at the Service of Hydroxide Transport across Phospholipid Bilayers. *J. Am. Chem. Soc.* **2024**, *146*, 7146−7151.

(50) (a) Rubini, P.; El Alaoui, H.; Abdallaoui, E. Determination of the ^{31}P NMR Chemical Shielding Tensor Anisostropy of Some Molecules in Solution. *Phosphorus, Sulfur Silicon Relat. Elem.* **1994**, *97*, 57−61. (b) Hargé, J.-C.; Abdallaoui, H. E. A. E.; Rubini, P. Interaction of phosphorylated molecules with protic solvents and cations. Discussion of the electronic perturbation at the phosphoryl bond of triphenyl-phosphine oxide. *Magn. Reson. Chem.* **1993**, *31*, 752−757.

(51) Herzfeld, J.; Berger, A. E. Sideband intensities in NMR spectra of samples spinning at the magic angle. *J. Chem. Phys.* **1980**, *73*, 6021−6030.

(52) Künzler, S.; Rathjen, S.; Merk, A.; Schmidtmann, M.; Müller, T. An Experimental Acidity Scale for Intramolecularly Stabilized Silyl Lewis Acids. *Chem. - Eur. J.* **2019**, No. 25, 15123−15130.

(53) Erdmann, P.; Leitner, J.; Schwarz, J.; Greb, L. An Extensive Set of Accurate Fluoride Ion Affinities for p-Block Element Lewis Acids and Basic Design Principles for Strong Fluoride Ion Acceptors. *ChemPhyschem* **2020**, *21*, 987−994.

(54) Erdmann, P.; Greb, L. Multidimensional Lewis Acidity: A Consistent Data Set of Chloride, Hydride, Methide, Water and Ammonia Affinities for 183 p-Block Element Lewis Acids. *ChemPhyschem* **2021**, *22*, 935−943.

(55) Jupp, A. R.; Johnstone, T. C.; Stephan, D. W. The global electrophilicity index as a metric for Lewis acidity. *Dalton Trans.* **2018**, *47*, 7029−7035.

https://doi.org/10.1021/jacs.5c17621
J. Am. Chem. Soc. 2026, 148, 14768−14778